Observed interactions between black carbon and hydrometeor during wet scavenging in mixed-phase clouds

Shuo Ding[1], Delong Zhao[2,8,9*], Cenlin He[3], Mengyu Huang[2,8,9], Hui He[2,8,9], Ping Tian[2,8,9], Quan Liu[2,8,9], Kai Bi[2], Chenjie Yu[4], Joseph Pitt[4], Ying Chen[5], Xincheng Ma[2,], Yunbo Chen[2], Xingcan Jia[7], Shaofei Kong[6], Jian Wu[6], Dawei Hu[4], Kang Hu[1], Deping Ding[2,8,9], Dantong Liu[1*]

1 Department of Atmospheric Sciences, School of Earth Sciences, Zhejiang University, Hangzhou, China
2 Beijing Weather Modification Office, Beijing, China
3 Advanced Study Program and Research Applications Laboratory, National Center for Atmospheric Research, Boulder, CO, USA
4 Centre for Atmospheric Sciences, School of Earth and Environmental Sciences, University of Manchester, Manchester M13 9PL, UK
5 Lancaster Environment Centre, Lancaster University, Lancaster LA1 4YQ, UK
6 Department of Atmospheric Sciences, School of Environmental Studies, China University of Geosciences (Wuhan), Wuhan, China
7 Institute of Urban Meteorology, Chinese Meteorological Administration, Beijing, China
8 Beijing Key Laboratory of Cloud, Precipitation and Atmospheric Water Resources, Beijing, China
9 Field experiment base of cloud and precipitation research in North China, China Meteorological Administration, Beijing, China

Key points:

This study provides the first detailed and continuous observations of black carbon interaction with mixed-phased clouds

In-cloud scavenging by droplets preferentially removes larger and thickly-coated black carbon

Black carbon with a larger core size in water droplets is released back to air through the WBF process during a snow event

Abstract

Wet scavenging of black carbon (BC) has been subject to large uncertainty, which importantly determines its atmospheric lifetime and indirect forcing impact on cloud microphysics. This study reveals the complex BC-hydrometeor interactions in mixed-phase clouds via single particle measurements in the real-world environment, by capturing precipitation processes throughout cloud formation, cold rain/graupel and subsequent snow events at a mountain site influenced by anthropogenic sources in wintertime. We found highly efficient BC wet scavenging during cloud formation, with large and thickly-coated BC preferentially incorporated into droplets. During snow processes, BC core sizes in the interstitial phase steadily increased. A mechanism was proposed whereby the BC mass within each droplet was accumulated through droplet collision, leading to larger BC cores, which were then released back to the interstitial air through the Wegener-Bergeron-Findeisen processes when ice dominated. These results provide fundamental basis for constraining BC wet scavenging.

Plain Language Summary

The wet removal of black carbon (BC) is crucial to determine its atmospheric lifetime and indirect radiative effects. However, the mechanism of BC-cloud particle interactions is still largely unknown, especially for mixed-phase clouds. This study conducted in-situ single particle measurements to reveal this microphysical process throughout an entire precipitation event. The BC particles with large core sizes and thick coatings were observed to be preferentially incorporated into liquid droplets when the cloud was formed. The subsequent droplet collision further resulted in fewer but larger droplets with larger BC cores inside. Afterwards, when a significant amount of ice was present, the water vapor could be transferred from droplets to ice crystals. As a result, the BC contained in the droplet could be released back to the interstitial phase, leading to larger BC cores in the air than those before the precipitation event.

This is an important process when considering the wet scavenging of BC in mixed-phase clouds, which is first observed in the real atmosphere in this study.

Key words: Black carbon, wet scavenging, WBF process, aerosol-cloud interaction

1 Introduction

Black carbon (BC) is strongly absorbing in the visible and near-infrared, which has an important radiative impact on regional and global scales [*T. C. Bond et al.*, 2013]. Because freshly emitted BC is highly water insoluble (hydrophobic), so it is hard for it to act as cloud condensation nuclei (CCN) [*Weingartner et al.*, 1997]. However, BC will show more hygroscopicity at sub-saturation if coated with water-soluble materials [*Andreae and Rosenfeld*, 2008; *Dusek et al.*, 2006; *D Liu et al.*, 2013], and in such cases may serve as CCN [*Kuwata et al.*, 2007].This is a crucial process to determine its atmospheric lifetime because of the subsequent cloud-precipitation removal [*Latha et al.*, 2010]. BC can be scavenged by in-cloud removal [*Sellegri*, 2003] and below-cloud scavenging [*Feng*, 2007] depending on its size and hygroscopicity. The in-situ measurements found that particles containing larger refractory BC (rBC) cores were preferentially removed by liquid cloud, consistent with Köhler theory [*N Moteki et al.*, 2012]. The CCN activity of BC associated with its mixing state has been computed in process models [*Fierce et al.*, 2015] or global models [*Oshima and Koike*, 2013] to quantify the ageing and removal time scale of BC in the atmosphere. However, this process is complicated by mixed-phase cloud. Long-term measurements at the Jungfraujoch alpine site showed that the aerosol scavenging efficiency, including BC, decreased with increased ice content of mixed-phase cloud [*Cozic et al.*, 2007; *Verheggen et al.*, 2007]. It is proposed that the Wegener-Bergeron-Findeisen (WBF) process may play an important role on releasing some of the aerosols contained in droplets. Because of the higher supersaturation over ice than liquid, the ice can thus grow at the cost of the water content in droplets by vapor deposition. Previous modelling studies suggested a large quantity of CCN will be released through the WBF process which acts to compensate for aerosol scavenging [*Schwarzenböck et al.*, 2001]. Accounting for the relatively low scavenging rate of BC in mixed-phase/ice clouds dominated by the WBF process will significantly improve the agreement between model results and observations [*Qi et al.*, 2017b], especially for the high-latitude Arctic region [*Qi et al.*, 2017a].

The importance of understanding the mechanism of BC wet deposition is not only to determine its atmospheric lifetime and thereby the global budget [*Koch et al.*, 2009], but also its indirect and semi-direct impacts on cloud properties [*Koch and Del Genio*, 2010]. The indirect radiative impact of BC by interacting with cloud is evaluated to be more important than its direct effect [*Wang*, 2013]. However the current parameterization of BC wet scavenging is still subject to significant uncertainty leading to large model-observation discrepancies [*J P Schwarz et al.*, 2010; *Sharma et al.*, 2013]. There is currently a lack of in-field detailed observations to explain and quantify the interactions between BC and cloud particles at the microscale, which hinders a better knowledge of the physical process.

This study chose a mountain site around Beijing city, which is substantially influenced by anthropogenic BC sources. A precipitation event was captured spanning a full cloud phase evolution from cloud formation to cold rain/graupel and subsequent snow process. This provides the first detailed and continuous observations of BC evolution during in-cloud scavenging in mixed-phase clouds in the real-world atmosphere.

2 Experimental site, instrumentation and data analysis

The mountain research station (hereinafter Yan station) in this study (115.78°E， 40.52°N, 1344 m above sea level) is located on the north of Taihang ridge to the northwest of Beijing. The site frequently experiences land contact of clouds and precipitation. This observation was conducted in the period 19th-21st Nov 2016, during the topographic precipitation and integrated cloud-seeding experiments (TOP-ICE, *X MA et al*., 2017). The temperature was mostly below zero and precipitation was in the form of graupel or snow. Besides Yan station, precipitation data was also collected from two other monitoring stations, Chang and Xi, located on the east (300 m) and southeast of Yan (500 m) respectively. The ground observation of BC physical properties in central Beijing was also conducted during the APHH project [*D Liu et al.*, 2018] at the same time as the experiment here.

In this study, the physical properties of BC particles were characterized using a single particle soot photometer (SP2, DMT Inc.) [*D Liu et al.*, 2010; *J Schwarz et al.*, 2006]. The SP2 incandescence signal was calibrated for refractory BC (rBC) mass using Aquadag® black carbon particle standards (Acheson Inc.,) and corrected for ambient rBC with a factor of 0.75 [*Laborde et al.*, 2012]. The mass-equivalent diameter of the rBC core (D_c) is obtained from the measured rBC mass assuming a density of 1.8 g m^{-3} [*Tami C Bond and Bergstrom*, 2006]. For a given time window, the mass median dimeter (MMD) of rBC core is calculated from the D_c distribution below and above which the rBC mass was equal. The coated BC size (D_p) is obtained by applying the Mie-look up table to match the core-shell modelled scattering cross section with measurement [*D Liu et al.*, 2014; *J W Taylor et al.*, 2015]. The SP2 laser power was monitored by the scattering peak amplitude of mono-dispersed PSL and showed very stable performance (within ±3%) during the experiment. The lack of SP2 data during certain periods was due to a hard drive issue of the data acquisition computer which did not affect the data quality. The bulk relative coating thickness (D_p/D_c) in a given time window is calculated as the total volume of coated BC particles divided by the total volume of the rBC cores, given by

$$\frac{D_p}{D_c} = \sqrt[3]{\frac{\sum_i D_{p,i}^3}{\sum_i D_{c,i}^3}} \qquad (1),$$

where $D_{p,i}$ and $D_{c,i}$ are the coated and rBC diameters for each single particle, respectively. The mass ratio of coating and rBC in bulk ($M_{coating}/M_{rBC}$) could be also obtained by assuming a density of coating 1.3 g cm^{-3} [*Cross et al.*, 2007] and rBC 1.8 g cm^{-3} [*Tami C Bond and Bergstrom*, 2006].

The droplet size distribution was measured by a Fog Monitor (model FM-100, DMT Inc) with optical diameter ranging from 2-50 μm [*Tav et al.*, 2018]. The precipitation was characterized by a Parsivel raindrop spectrometer [*Löffler-Mang and Joss*, 2000] with a forward-scattering optical system to collect precipitation particles and output the particle size and velocity, ranging from 0.2-25 mm and 0.2-20 m/s respectively. In addition, the meteorological parameters including temperature, RH and wind were continuously measured at Yan, with a visibility sensor (Belfort Model 6000, visual range: 200 m–50 km) to monitor the atmospheric visibility. Meanwhile, the images of precipitation particles were also obtained by photomicrography.

The HYSPLIT 4.0 model [*Draxler et al.*, 1997] using $1^{\circ}\times1^{\circ}$, 3-hourly GDAS1 reanalysis was used to calculate back trajectories, aiding identification of the source locations. The model performed ensemble simulations with 27 trajectories for each run. In addition, the NAME (the Numerical Atmospheric-dispersion Modelling Environment) model [*Jones et al.*, 2007] using meteorological data from the global configuration of the UK Met Office's Unified Model was employed to obtain air histories quantifying the relative influence of emissions from different regions. The model was run in backwards mode, releasing tracer particles from the Yan measurement site and recording the integrated time spent by these tracer particles in the lowest 0-1000m a.g.l. on a 0.25° × 0.25° horizontal grid, aggregated over all particles for a given release period. Tracer particles were released at a nominal rate of 1 g/s, with a maximum travel time of 48 hours (i.e. the air histories represent the relative influence of different regions on the sampled air over the 2 days prior to measurement at Yan station).

All aerosols were sampled from a $PM_{2.5}$ impactor (BGI SCC1.829), which means most of the cloud particles will be screened out and the sampled particles will represent the interstitial phase between cloud particles.

Besides the experiment in Nov. 2016, another identical experiment was conducted in Mar. 2019. Along with the measurements from the main sampling line, scanning electron microscope (SEM) analysis was performed for particles collected on the copper grids coated with carbon film (carbon type-B, 300-mesh copper, Tianld Co., China) [*Xu et al.*, 2019]. For the SEM samples, a $PM_{2.5}$ cascade impactor was applied during the snowing period, but without being applied during the fog period in order to collect both interstitial and in-cloud particles.

4 Results and discussions

4.1 In-cloud scavenging of BC

As Figure 1 shows, this experiment spanned a full precipitation process including cloud formation, cold rain/graupel and subsequent snow precipitation. The BC properties in the interstitial phase (out of hydrometeor) were monitored throughout the period. Five periods were defined: Dry (without hydrometer), A (BC accumulation), B (droplet formation and BC scavenging), C (graupel formation) and D period (snow and BC releasing). Only the Dry period had RH < 60% and an absence of hydrometeors with visibility > 9 km, and periods B-D all had very high relative humidity with visibility < 5 km. In the Dry period, BC had a relatively low mass loading (384.8±384.4 ng m^{-3}), a stable D_c at 0.21±0.01μm and the coatings maintained at 0.043±0.04 μm. The HYSPLIT back-trajectories (Figure A2) showed a uniform northwesterly air mass with occasional land contact. The NAME dispersion model (Figure A3) showed the recent surface influence on the air mass was relatively low, consistent with the lower BC concentration during this period. The MODIS visible cloud images (Figure A4) also showed clear sky over the site in Dry period, but the emergence of ice clouds from period A that intensified in period D. Ground precipitation was also observed from period C (Figure 1b).

Period A represented the initial formation of droplets, although unfortunately the fog monitor suffered a data outage for most of this period. However, the high RH coincident with a decrease of visibility indicates fog droplets started to form, but did not reach a large enough size to be impacted by the $PM_{2.5}$ inlet. This period showed significant increase in BC concentration (Figure 1g) and BC coating thickness (Figure 1f), indicating the BC mass from south/southeast sources had not been significantly scavenged. There was some variability of BC mass loadings; however the BC core size (Figure 1e) remained stable at 0.20μm. The ensemble backtrajectories (Figure A2b) indicated that the sampled air was influenced by high BC emissions to the south/southeast, although in this model the trajectories were mostly still northwesterly because of Mongolian high-pressure system. In contrast, the NAME air histories (Figure A3b-e) indicated that through period A-D, the low-level contribution was mainly from south/southeast and in period D this surface contribution was lessened. This was in line with the BC emission inventory (Figure A3f), which shows that significant anthropogenic BC emission was present to the southeast of the experimental site. Combing with the Dry period, period A clearly showed a highly stable BC core size when BC was not subject to significant scavenging at this initial stage, despite the variation of BC mass loading, and this constant median D_c is shown by a dash line in Figure 1e. Given that the BC core size may reflect the source profile [*D Liu et al.*, 2014; *J Schwarz et al.*, 2008], this implies BC sources were stable during the experimental period.

Period B was the time when droplet started to appreciably form. During this process, the effective diameter (D_{eff}; i.e., area-weighted mean diameter) of droplets was growing from 4.9 μm to 13.8 μm, but the number concentration of droplets decreased by 80% in about 7 hours. Figure A5 also shows a negative correlation between droplet number concentration and D_{eff}. This suggests a collision process of droplets leading to the increase in droplet sizes [*Kollár et al.*, 2005]. Precipitation was not observed during this period (Figure 1b). Note that the increase of liquid water content (LWC) exactly coincided with the decrease in BC mass/number concentration, median D_c, coatings and coated BC size. This means an efficient in-cloud scavenging of BC began as soon as droplets were formed. In line with Köhler theory, the observations here revealed that the larger particles, i.e. the larger BC-containing particles with larger core sizes and thicker coatings, were preferentially removed by droplets, leading to BC with smaller cores and less coating in the interstitial phase, which is consistent with previous in-situ measurements [*N. Moteki et al.*, 2012; *J Taylor et al.*, 2014]. During this period, ~75% of the rBC mass was scavenged. Median D_c decreased from 0.2 μm to 0.16 μm and remained at this size when rBC mass loading reached its lowest value of 170 ng m^{-3}.

It should be noted that due to collision of droplets, the BC cores incorporated in each droplet could be merged in one larger droplet, thus multiple BC cores could be contained in one collided droplet as has been revealed by a recent microscopy study [*L Liu et al.*, 2018]. The merged BC cores in collided droplets could further coagulate and lead to an enlargement of BC core sizes. A conceptual model analysis (detailed in the Supplement) was conducted to quantitatively understand the BC size enlargement in the droplets during collision processes. The model analysis is consistent with the observation here when considering ~80% of the droplets participated in the collision process.

4.2 BC interaction with graupel or snow

During the period C, precipitation on the ground started to be observed. Droplet number concentration remained almost constant while LWC was considerably lower compared to the period B. The precipitation particles seen from microscopy (Figure 1 middle) mainly showed the form of graupel with significant riming of supercooled droplets (temperature ~ -5°C). The precipitation during this period had a peak diameter at 1 mm and also contained the other mode of larger particles spanning from

1.5-4 mm (Figure A5d). The mean falling velocity for the graupel size of 2-4 mm was relatively high at 3±1.2m s^{-1}. As Figure 1d showed, the increase in precipitation rate corresponded with the decrease in LWC. Contrasting to the period B, the droplets in the period C showed relatively constant number concentrations with a short gap, after which the second fog event showed a smaller D_{eff} and lower LWC. The rimming of LWC by graupel was thus deemed to be the main process of keeping low levels of LWC and droplet number concentration [*Ávila et al.*, 2009]. The BC concentration remained low (<190 ng m^{-3}) from the initialization of precipitation until the precipitation rate reached the maximum, suggesting the scavenging activity by the graupel was still high. In the late stage of period C, the fog began to vanish and the continuous contribution of BC sources to the site (according to NAME model) tended to introduce more coated BC without being scavenged. The BC core size in the interstitial air started to increase towards the end of period C when precipitation rate started to decrease (note that there was a short period lasting about 1 hour with decreasing D_c which corresponded with the increase in LWC for that short period).

During the period D, LWC was as low as 1.6×10^{-4} g m^{-3} throughout the period with increased D_{eff} for the second half. The precipitation at the Yan site was weak for the first half of the period but the precipitation of heavy snowflakes (image shown by microscopy, Figure 1) started from 4 am. The lower precipitation rate during the first half was observed at the other two sites (Chang and Xi) to the east and southeast of Yan (Figure 1b). The visibility was slightly higher than period C due to reduced droplet concentration. Figure A6 showed that for hydrometeor particle diameters of 2-4 μm, the snowflake precipitation falling speed at 2±0.3 m s^{-1} was lower than that of the graupel in period C. The significant fraction of small hydrometeor particles (Figure A6) was because of the shattering of falling snowflakes [*Mossop*, 1985].

The first half of the period D was when the BC concentration started to increase and median D_c started to be above the reference line (205nm) for ambient BC before being scavenged (the dash line in Figure 1e). This period was the time before the heavy snow precipitation formed, with very low LWC but high RH and low visibility. The cloud glaciation may have occurred during this period (though a lack of cloud microphysics observation over the site makes it difficult to draw concrete conclusions) with ice growth consuming the LWC, but the particles may have not reached the size large enough to be detected by the precipitation instrument. The BC core size maintained the steadily increasing trend from 0.20 μm to 0.26 μm throughout the period D, which lasted over 8 hours. The BC concentration varied in this period from 70 ng m^{-3} to 508 ng m^{-3}.

One of the hypotheses here is the increase of D_c may result from additional sources, which may be a new source or preexisting (but being modified) source. However, this hypothesis was firmly excluded based on the following reasons. Firstly, the NAME dispersion model showed a weakened source contribution from the most intensive emission region to the southeast of the site. In addition, any burning was strictly prohibited within ~5km around the site because of the fire regulation on the forest-covered mountain. In addition, period D spanned the time from close to midnight to early morning, when the planetary boundary layer (PBL) was not likely to be elevated high enough to advect the pollutants from lower level to the mountain site. Furthermore, the new source had to last continuously for over 8 hours in order to contribute to the continuous increase of D_c, which is very unlikely in this case. To further support the discussion, we also compared the results here with the ground measurements conducted in urban Beijing for one month at the same time (during Nov.-Dec. 2016). As Figure 2b shows, during this one-month experiment, experiencing sources for all air mass directions and meteorological conditions, there was no appreciable BC with D_c over 0.22 μm, whereas period D showed substantial increase of D_c above 0.22 μm. In other periods the pattern (D_c vs BC mass) fell within the range of ground measurements.

Therefore, we conclude that the enlargement of BC core size was from the existing BC particles which had been included in the droplets (period B), but were then released back to air in period D when ice or snow grew through the deposition of water vapor that transfers from liquid to ice (i.e., WBF process). This WBF process was more likely to occur in period D than in C because of the lower hydrometeor falling speed (Figure A6). The multiple BC cores in the droplet must have been processed and modified to be significantly larger than the reference ambient $D_{c,}$ resulting in a larger size distribution than the ambient. This process is consistent with the view that the drop collision could merge the BC cores in multiple droplets into the same one (part 1 of model validation in Supplement), and then became one larger BC core after the droplet was evaporated, also evidenced by SEM results shown in Figure 3. The start of period D had a higher BC mass loading, which may result from a higher initial rate of release. According to the Kelvin effect [*Krarnes et al.*, 1991] in cloud microphysics, smaller droplets (containing smaller D_c) will evaporate first and larger droplets (containing larger D_c) follow, which explains why D_c maintained the increasing trend (part 2 of model validation in Supplement). Interestingly, the released BC had a steadily but slightly decreased coating content per unit rBC mass during the releasing process (Figure 1f). This is because a portion of the BC coatings could dissolve into the droplet medium and evaporate along with the droplet evaporation (e.g. [*Ervens et al.*, 2011; *Galloway et al.*, 2014; *Zardini et al.*, 2010]). As a result, the released BC contains less coatings as before. The proposed mechanism of interactions between BC and hydrometeors is schematically summarized in Figure 3.

Based on another set of identical measurements during precipitation events experienced in springtime 2019 (Figure A8), a notable decrease of Dc by 20% was also observed on 10th Mar. during the cloud formation (with ~50% decrease of rBC mass), followed by an increase of D_c above the ambient D_c size during snow (Figure 2a). This event replicated the preceding longer precipitation event in 2016 when the cloud and snow also occurred in sequence. During another event on 9th Mar. 2019, however, D_c did not exhibit marked variation, along with an insignificant BC scavenging. This may be due to the overlap of cloud formation and snow periods, leading to a co-occurrence of decrease and enhancement of D_c. Thus, based on the observed 2019 events (particularly the 10th Mar. event), we further validate the conclusion derived from the preceding 2016 events for the efficient BC in-cloud scavenging and subsequent BC releasing driven by the WBF process.

The microstructure of BC from SEM during the 10^{th} Mar. 2019 event further validates the proposed mechanism demonstrated in Figure. 3. Before cloud formation, most of the detected single particles were at maximum projected diameter (D_{max}) of 200-500nm and mostly in a shape of open cluster and no compact shape was observed. During cloud formation, more larger BC particles were observed (D_{max} >450nm) in high fluffy shape. Note that there was no $PM_{2.5}$ impactor installed during this period, both particles within and outside of droplets may have been measured. During snow (with impactor), there was an appreciable number of compact and large (D_{max} >500nm) BC observed in the interstitial phase, and they were in notably high compact shapes. Such amount of BC in compact shape was not observed for the other time before the precipitation event. This strongly supports the cloud-accumulation and subsequent snow-releasing mechanism illustrated in Fig. 3.

4.3 The scavenging and releasing rates of BC as a function of core size

The lognormal distribution of BC core size for each period (A~D) is shown in Figure 2. The scavenging rate of BC (R_{sca}) as a function of core size is calculated as the difference in size distribution between period A and B relative to A: (B-A)/A. Here we assume the variation in rBC mass loading in period A represents the general variation of ambient BC as the source contribution was similar between period A and B (Figure A3). The releasing rate ($R_{release}$) is calculated as the difference between D and C relative to C: (D-C)/C. An exponential relationship between BC scavenging/releasing rate and core size is found as $R_{sca}=0.95-0.60\exp(-10.24*D_c)$ and $R_{release}=6.16-7.11\exp(-0.79D_c)$.

A conceptual model analysis (detailed in the Supplement) has been proposed to quantitatively reproduce the observed exponential relationship between the BC core size and scavenging/releasing rate by applying a first-order BC in-cloud scavenging/releasing scheme [*H Liu et al.*, 2001; *Neale et al.*, 2010], expressed as:

$$[BC]_{scav/rel} = [BC]_0 F(1 - e^{-k\Delta t}) \qquad (2),$$

where $[BC]_{scav/rel}$ denotes scavenged/released BC mass concentration, and $[BC]_0$ denotes BC mass concentration in the air before scavenging or in clouds before releasing. F is the areal fraction of the cloudy region where the scavenging/releasing process takes place, and k represents the first-order BC in-cloud scavenging (k_s) or releasing (k_r) rate parameter. The observed relationship between scavenging/releasing rate and BC core sizes infers a linear relationship between k (i.e., k_s or k_r) and D_c. Thus, an observation-constrained $k_s = 9.48\times10^{-4} D_c + 4.25\times10^{-5}$ is obtained, and the resulting in-cloud scavenging rate parameter (k_s) is 0.9×10^{-4} ~ 0.5×10^{-3} s^{-1} for a typical D_c range of 0.05–0.5 μm (see Supplement for details). Note that k_s obtained here is for thin orographic cloud with LWC up to $0.1 gm^{-3}$, and this is generally consistent with, but slightly smaller than, the typical values (10^{-4}~10^{-3} s^{-1}) used for the stratiform warm cloud condition in global models (e.g., H. Liu et al., 2001). Previous studies (e.g., Qi et al., 2017a,b) have shown that the k_s tends to be smaller in mixed-phase clouds dominated by the WBF process. Similarly, an observation-constrained $k_r = 5.5\times10^{-5} D_c - 1.0\times10^{-5}$ is obtained, leading to a releasing rate parameter (k_r) of up to 1.8×10^{-5} s^{-1} for D_c values of up to 0.5 μm. We note that the aforementioned conceptual model analyses are simplified and only used here to quantitatively understand the observed relationship between BC scavenging/releasing rate and core sizes. More accurate estimates and comparisons with observations require a more sophisticated aerosol-cloud size-resolved model, which will be investigated in future studies. Nevertheless, our analysis suggests that the observations in this study are very useful to improve and constrain BC wet scavenging schemes in models.

Conclusions

A full process of interactions between BC and hydrometeors was observed in this study, as schematically illustrated in Figure 3. The larger and thickly coated BC was observed to be efficiently removed by cloud droplets. The phenomenon of BC release from pre-existing liquid droplets during ice/snow particle formation was observed for the first time at the micro-scale; this emphasizes the importance of the presence of ice on reducing the scavenging rate of BC [*Schwarzenböck et al.*, 2001]. A mechanism was proposed whereby BC particles are accumulated by droplet collision before being released back to air in a more aggregated form (with larger cores) during the WBF process. All these processes could explain the variation of BC core size distribution observed across various locations or under different meteorological conditions.

The mechanism proposed here, such as efficient in-cloud removal of larger BC with thicker coatings, BC particle aggregating during droplet collision/merging, and subsequent BC releasing driven by the WBF processes, has wide applications in conditions when ice or mixed-phase clouds dominate coexisting water droplets. This may explain large model-measurement discrepancies such as the underestimates of BC concentration at high latitude and altitude areas dominated by mixed-phase or ice clouds [*He et al.*, 2014; *Qi et al.*, 2017a]. The BC core size-dependent in-cloud scavenging and releasing rates as observed in this study could be used to constrain a range of modelling activities.

Acknowledgments

This research was supported by the National Key Research and Development Programme of China (2016YFA0602001), National Natural Science Foundation of China (41605108,41875044,41775138,41875167,41675138), National Science Foundation of Beijing (8172023). C. He was supported by the NCAR Advanced Study Program (ASP) Fellowship. The National Center for Atmospheric Research (NCAR) is sponsored by the National Science Foundation (NSF). We acknowledge use of the NAME atmospheric dispersion model and associated NWP meteorological data sets made available to us by the Met Office. We acknowledge the significant storage resources and analysis facilities made available to us on JASMIN by STFC CEDA

along with the corresponding support teams. Processed data is available from the file sharing link (https://pan.baidu.com/s/1YqnLHZly24URgULZ-HIlOw) using extracting code u457.

References

Andreae, M. O., and D. Rosenfeld (2008), Aerosol–cloud–precipitation interactions. Part 1. The nature and sources of cloud-active aerosols, *Earth-Science Reviews*, *89*(1-2), 13-41.

Ávila, E. E., N. E. Castellano, C. P. R. Saunders, R. E. Bürgesser, and G. G. Aguirre Varela (2009), Initial stages of the riming process on ice crystals, *Geophysical Research Letters*, *36*(9).

Bond, T. C., and R. W. Bergstrom (2006), Light absorption by carbonaceous particles: An investigative review, *Aerosol Sci. Tech.*, *40*(1), 27-67.

Bond, T. C., et al. (2013), Bounding the role of black carbon in the climate system: A scientific assessment, *Journal of Geophysical Research: Atmospheres*, *118*(11), 5380-5552.

Cozic, J., B. Verheggen, S. Mertes, P. Connolly, K. Bower, A. Petzold, U. Baltensperger, and E. Weingartner (2007), Scavenging of black carbon in mixed phase clouds at the high alpine site Jungfraujoch, *Atmos. Chem. Phys.*, *7*(7), 1797-1807.

Cross, E. S., J. G. Slowik, P. Davidovits, J. D. Allan, D. R. Worsnop, J. T. Jayne, D. K. Lewis†, M. Canagaratna, and T. B. Onasch (2007), Laboratory and ambient particle density determinations using light scattering in conjunction with aerosol mass spectrometry, *Aerosol Sci. Tech.*, *41*(4), 343-359.

Draxler, R. R., G. D. Hess, and R. R. Draxler (1997), DESCRIPTION OF THE HYSPLIT_4 MODELING SYSTEM, paper presented at National Oceanic & Atmospheric Administration Technical Memorandum Erl Arl.

Dusek, U., G. P. Reischl, and R. Hitzenberger (2006), CCN activation of pure and coated carbon black particles, *Environmental Science & Technology*, *40*(4), 1223-1230.

Ervens, B., B. J. Turpin, and R. J. Weber (2011), Secondary organic aerosol formation in cloud droplets and aqueous particles (aqSOA): a review of laboratory, field and model studies, *Atmospheric Chemistry and Physics*, *11*(21), 11069-11102.

Feng, J. (2007), A 3-mode parameterization of below-cloud scavenging of aerosols for use in atmospheric dispersion models, *Atmospheric Environment*, *41*(32), 6808-6822.

Fierce, L., N. Riemer, and T. C. Bond (2015), Explaining variance in black carbon's aging timescale, *Atmospheric Chemistry and Physics*, *15*(6), 3173-3191.

Galloway, M. M., M. H. Powelson, N. Sedehi, S. E. Wood, K. D. Millage, J. A. Kononenko, A. D. Rynaski, and D. O. De Haan (2014), Secondary Organic Aerosol Formation during Evaporation of Droplets Containing Atmospheric Aldehydes, Amines, and Ammonium Sulfate, *Environmental Science & Technology*, *48*(24), 14417-14425.

He, C., Q. B. Li, K. N. Liou, J. Zhang, L. Qi, Y. Mao, M. Gao, Z. Lu, D. G. Streets, and Q. Zhang (2014), A global 3-D CTM evaluation of black carbon in the Tibetan Plateau, *Atmospheric Chemistry & Physics*, *14*(13), 7091-7112.

Jones, A., D. Thomson, M. Hort, and B. Devenish (2007), The U.K. Met Office's Next-Generation Atmospheric Dispersion Model, NAME III, Springer US, Boston, MA.

Koch, D., and A. D. Del Genio (2010), Black carbon semi-direct effects on cloud cover: review and synthesis, *Atmos. Chem. Phys.*, *10*(16), 7685-7696.

Koch, D., et al. (2009), Evaluation of black carbon estimations in global aerosol models, *Atmos. Chem. Phys.*, *9*(22), 9001-9026.

Kollár, L. E., M. Farzaneh, and A. R. Karev (2005), Modeling droplet collision and coalescence in an icing wind tunnel and the influence of these processes on droplet size distribution, *International Journal of Multiphase Flow*, *31*(1), 69-92.

Krarnes, J., H. Büttner, and F. Ebert (1991), Submicron particle generation by evaporation of water droplets, *Journal of Aerosol Science*, *22*(6), S15–S18.

Kuwata, M., Y. Kondo, M. Mochida, N. Takegawa, and K. Kawamura (2007), Dependence of CCN activity of less volatile particles on the amount of coating observed in Tokyo, *Journal of Geophysical Research*, *112*(D11).

Löffler-Mang, M., and J. Joss (2000), An optical disdrometer for measuring size and velocity of hydrometeors, *Journal of Atmospheric and Oceanic Technology*, *17*(2), 130-139.

Laborde, M., et al. (2012), Single Particle Soot Photometer intercomparison at the AIDA chamber, *Atmos. Meas. Tech.*, *5*(12), 3077-3097.

Latha, K. M., K. V. S. Badarinath, and P. M. Reddy (2010), Scavenging efficiency of rainfall on black carbon aerosols over an urban environment, *Atmospheric Science Letters*, *6*(3), 148-151.

Liu, D., J. Allan, J. Whitehead, D. Young, M. Flynn, H. Coe, G. McFiggans, Z. L. Fleming, and B. Bandy (2013), Ambient black carbon particle hygroscopic properties controlled by mixing state and composition, *Atmospheric Chemistry and Physics*, *13*(4), 2015-2029.

Liu, D., et al. (2014), Size distribution, mixing state and source apportionment of black carbon aerosol in London during wintertime, *Atmospheric Chemistry and Physics*, *14*(18), 10061-10084.

Liu, D., et al. (2018), Contrasting physical properties of black carbon in urban Beijing between winter and summer, *Atmos. Chem. Phys. Discuss.*, *2018*, 1-30.

Liu, D., et al. (2010), Single particle characterization of black carbon aerosols at a tropospheric alpine site in Switzerland, *Atmos. Chem. Phys.*, *10*(15), 7389-7407.

Liu, H., D. J. Jacob, I. Bey, and R. M. Yantosca (2001), Constraints from 210Pb and 7Be on wet deposition and transport in a global three - dimensional chemical tracer model driven by assimilated meteorological fields, *J. Geophys. Res. - Atmos.*, *106*(D11), 12109-12128.

Liu, L., et al. (2018), Cloud scavenging of anthropogenic refractory particles at a mountain site in North China, *Atmos. Chem. Phys.*, *18*(19), 14681-14693.

Mossop, S. C. (1985), The Origin and Concentration of Ice Crystals in Clouds, *Bulletin of the American Meteorological Society*, *66*(3), 264-273.

Moteki, N., Y. Kondo, N. Oshima, N. Takegawa, M. Koike, K. Kita, H. Matsui, and M. Kajino (2012), Size dependence of wet removal of black carbon aerosols during transport from the boundary layer to the free troposphere, *Geophys. Res. Lett.*, *39*(13).

Moteki, N., Y. Kondo, N. Oshima, N. Takegawa, M. Koike, K. Kita, H. Matsui, and M. Kajino (2012), Size dependence of wet removal of black carbon aerosols during transport from the boundary layer to the free troposphere, *Geophysical Research Letters*, *39*(13), L13802.

Neale, R. B., C.-C. Chen, A. Gettelman, P. H. Lauritzen, S. Park, D. L. Williamson, A. J. Conley, R. Garcia, D. Kinnison, and J.-F. Lamarque (2010), Description of the NCAR community atmosphere model (CAM 5.0), *NCAR Tech. Note NCAR/TN-486+ STR*, *1*(1), 1-12.

Oshima, N., and M. Koike (2013), Development of a parameterization of black carbon aging for use in general circulation models, *Geoscientific Model Development (GMD) & Discussions (GMDD)*.

Qi, L., Q. Li, Y. Li, and C. He (2017a), Factors controlling black carbon distribution in the Arctic, *Atmospheric Chemistry and Physics*, *17*(2), 1037-1059.

Qi, L., Q. Li, C. He, X. Wang, and J. Huang (2017b), Effects of the Wegener–Bergeron–Findeisen process on global black carbon distribution, *Atmospheric Chemistry and Physics*, *17*(12), 7459-7479.

Schwarz, J., R. Gao, D. Fahey, D. Thomson, L. Watts, J. Wilson, J. Reeves, M. Darbeheshti, D. Baumgardner, and G. Kok (2006), Single - particle measurements of midlatitude black carbon and light - scattering aerosols from the boundary layer to the lower stratosphere, *J. Geophys. Res. - Atmos.*, *111*(D16).

Schwarz, J., R. Gao, J. Spackman, L. Watts, D. Thomson, D. Fahey, T. Ryerson, J. Peischl, J. Holloway, and M. Trainer (2008), Measurement of the mixing state, mass, and optical size of individual black carbon particles in urban and biomass burning emissions, *Geophys. Res. Lett.*, *35*(13).

Schwarz, J. P., J. R. Spackman, R. S. Gao, L. A. Watts, P. Stier, M. Schulz, S. M. Davis, S. C. Wofsy, and D. W. Fahey (2010), Global-scale black carbon profiles observed in the remote atmosphere and compared to models, *Geophysical Research Letters*, *37*(18), L18812.

Schwarzenböck, A., S. Mertes, J. Heintzenberg, W. Wobrock, and P. Laj (2001), Impact of the Bergeron–Findeisen process on the release of aerosol particles during the evolution of cloud ice, *Atmospheric Research*, *58*(4), 295-313.

Sellegri, K. (2003), Size-dependent scavenging efficiencies of multicomponent atmospheric aerosols in clouds, *Journal of Geophysical Research, 108*(D11).

Sharma, S., M. Ishizawa, D. Chan, D. Lavoué, E. Andrews, K. Eleftheriadis, and S. Maksyutov (2013), 16-year simulation of Arctic black carbon: Transport, source contribution, and sensitivity analysis on deposition, *Journal of Geophysical Research: Atmospheres*, *118*(2), 943-964.

Tav, J., O. Masson, F. Burnet, P. Paulat, T. Bourrianne, S. Conil, and L. Pourcelot (2018), Determination of Fog-Droplet Deposition Velocity from a Simple Weighing Method, *Aerosol and Air Quality Research*, *18*(1), 103-113.

Taylor, J., J. Allan, G. Allen, H. Coe, P. Williams, M. Flynn, M. Le Breton, J. Muller, C. Percival, and D. Oram (2014), Size-dependent wet removal of black carbon in Canadian biomass burning plumes, *Atmos. Chem. Phys.*, *14*(24), 13755-13771.

Taylor, J. W., J. D. Allan, D. Liu, M. Flynn, R. Weber, X. Zhang, B. L. Lefer, N. Grossberg, J. Flynn, and H. Coe (2015), Assessment of the sensitivity of core / shell parameters derived using the single-particle soot photometer to density and refractive index, *Atmospheric Measurement Techniques*, *8*(4), 1701-1718.

Verheggen, B., J. Cozic, E. Weingartner, K. Bower, S. Mertes, P. Connolly, M. Gallagher, M. Flynn, T. Choularton, and U. Baltensperger (2007), Aerosol partitioning between the interstitial and the condensed phase in mixed - phase clouds, *J. Geophys. Res. - Atmos.*, *112*(D23).

Wang, C. (2013), Impact of anthropogenic absorbing aerosols on clouds and precipitation: A review of recent progresses, *Atmospheric Research*, *122*(3), 237-249.

Weingartner, E., H. Burtscher, and U. Baltensperger (1997), Hygroscopic properties of carbon and diesel soot particles, *Atmos. Environ.*, *31*(15), 2311-2327.

Xu, L., D. Zhang, and W. Li (2019), Microscopic comparison of aerosol particles collected at an urban site in North China and a coastal site in Japan, *Science of The Total Environment*, *669*, 948-954.

Zardini, A. A., I. Riipinen, I. K. Koponen, M. Kulmala, and M. Bilde (2010), Evaporation of ternary inorganic/organic aqueous droplets: Sodium chloride, succinic acid and water, *Journal of Aerosol Science*, *41*(8), 760-770.

Figures and captions

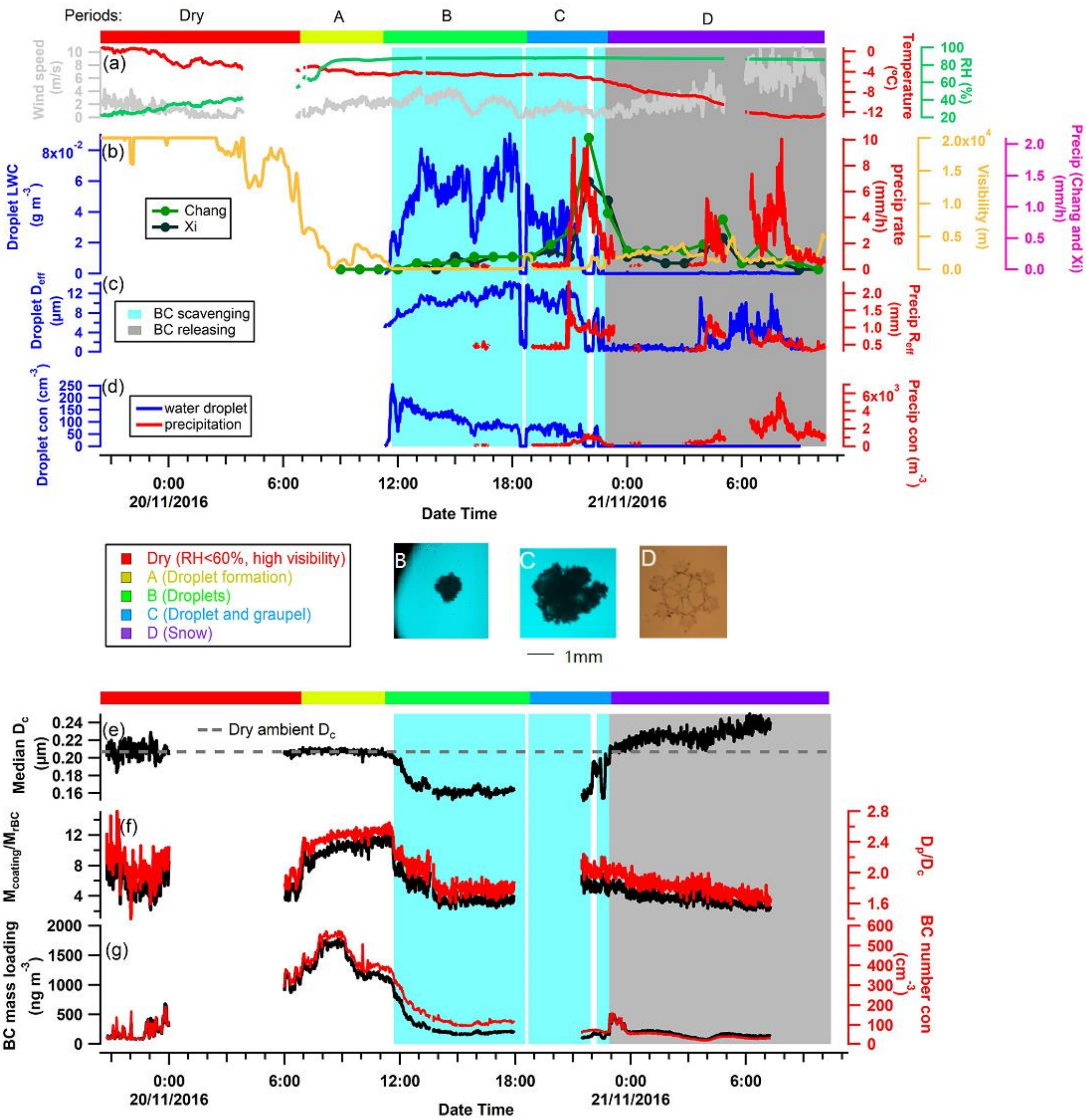

Figure 1. Time series of meteorology (panel a to d) and BC properties (panels e-g) during the experiment at Yan site. The color bar on top of panels indicates the defined periods, and blue and grey shades denote the periods with BC scavenging and releasing dominated a) related meteorology parameters RH, ambient temperature and wind speed. b) precipitation rate, liquid water content (LWC) and precipitation rate at Chang and Xi on the right axis. c) effective diameter of droplet and effective radius of precipitation d) droplet and precipitation number concentration. e) rBC core mass median diameter (Dc) with grey dashed line showing the Dc of dry ambient BC. f) $M_{coating}/M_{rBC}$ and bulk relative coating thickness D_p/D_c. g) BC mass and number concentration. Typical images of hydrometeor for B, C, D periods are shown in the middle.

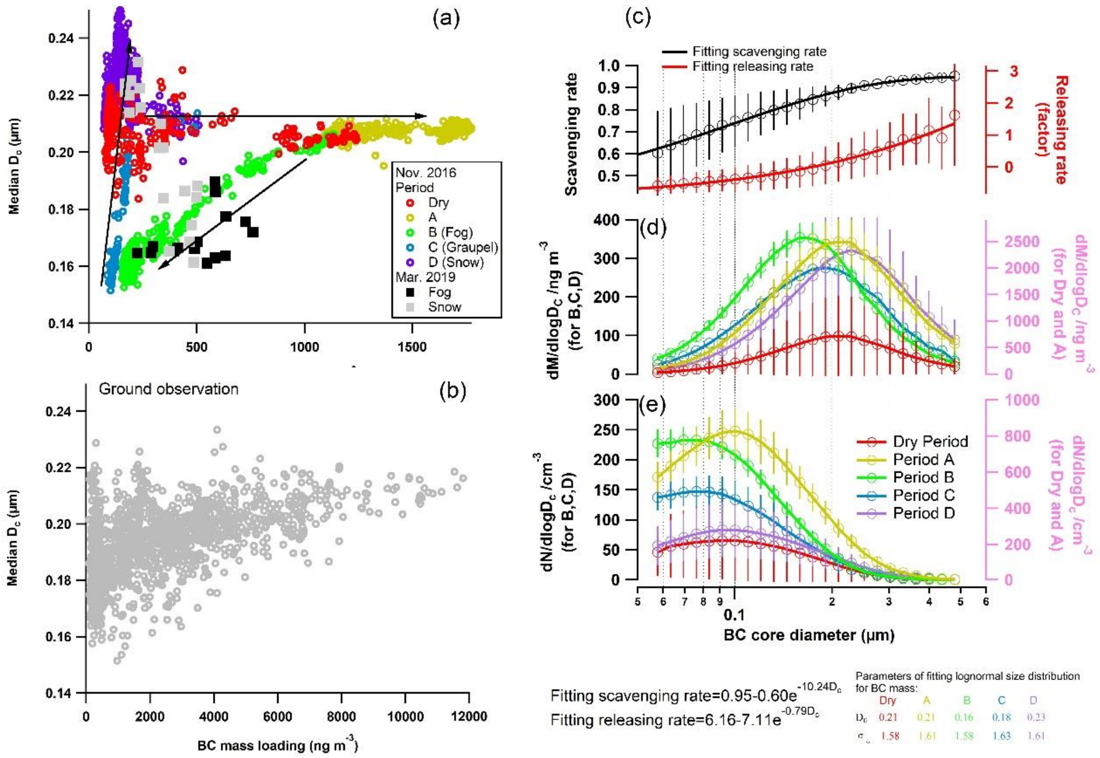

Figure 2. (a) rBC mass median core size diameter (median D_c) as a function of rBC mass loading for the precipitation events in Nov. 2016 and Mar. 2019. The arrows broadly indicate the temporal evolution for each period in Nov. 2016. (b) ground measurements [*D Liu et al.*, 2018] conducted in urban Beijing covering the same period with the mountain experiment. (c-e) Size distribution of BC core size for each period, with error bars showing ±standard deviation relative to mean. The parameters of lognormal fitting on dM/dlogD_c for each period is listed below (D_0 is the central diameter and σ_g is the geometric standard deviation). Panel (c) shows the scavenging rate (A relative to B), and releasing rate (D relative to C), with the exponential fitting functions marked below.

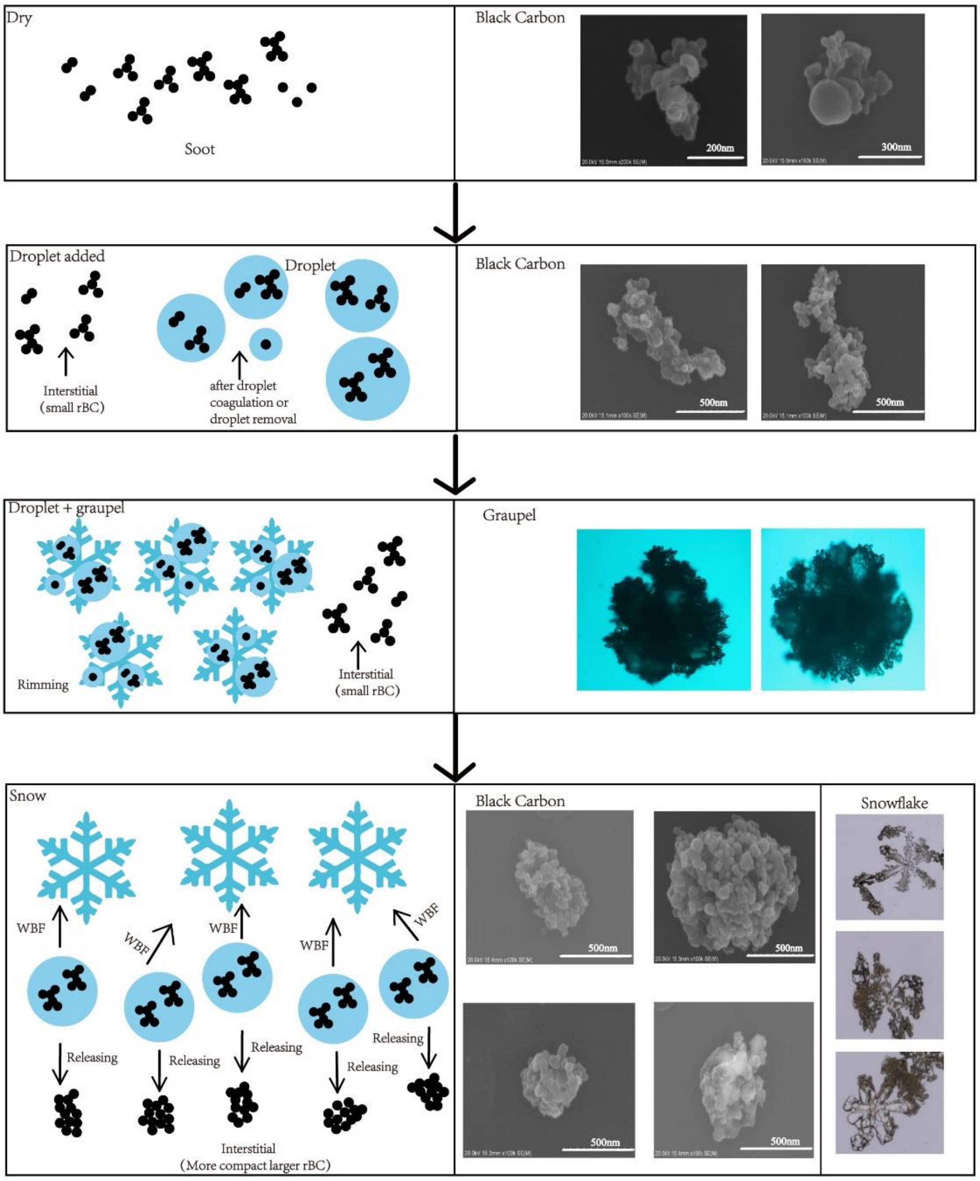

Figure 3. Schematic illustration of the interaction between BC and hydrometeors during different stages of scavenging processes. Right panels show the typical scanning electron microscope (SEM) images of single BC particles for each process, and the hydrometeor images (for graupel and snowflake) taken by photomicrography are shown for the precipitation stages.

Figure1.

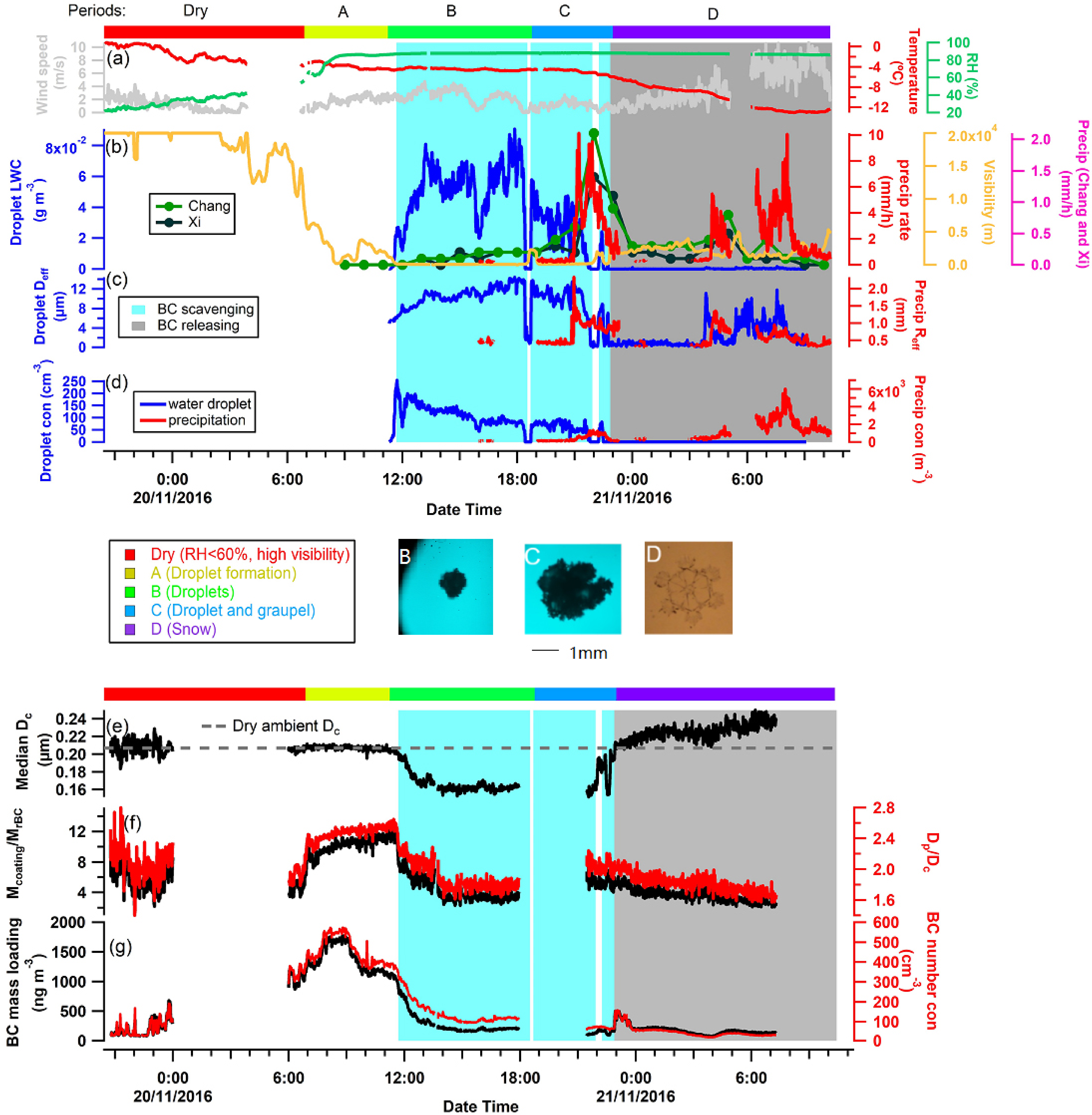

Periods: Dry A B C D
Wind speed (m/s)
Temperature (°C)
RH (%)
Droplet LWC (g m-3)
precip rate (mm/h)
Visibility (m)
Precip (Chang and Xi) (mm/h)
Chang
Xi
Droplet Deff (µm)
Precip Reff (mm)
BC scavenging
BC releasing
Droplet con (cm-3)
Precip con (m-3)
water droplet
precipitation
0:00 20/11/2016
6:00
12:00
18:00
0:00 21/11/2016
Date Time
Dry (RH<60%, high visibility)
A (Droplet formation)
B (Droplets)
C (Droplet and graupel)
D (Snow)
1mm
Median Dc (µm)
Dry ambient Dc
Mcoating/MrBC
Dp/Dc
BC mass loading (ng m-3)
BC number con (cm-3)

Figure2.

(a)
Median D_c (µm)
Nov. 2016
Period
Dry
A
B (Fog)
C (Graupel)
D (Snow)
Mar. 2019
Fog
Snow
Ground observation
(b)
BC mass loading (ng m^-3)
(c)
Fitting scavenging rate
Fitting releasing rate
Scavenging rate
Releasing rate (factor)
(d)
dM/dlogD_c /ng m^-3 (for B,C,D)
dM/dlogD_c /ng m^-3 (for Dry and A)
(e)
dN/dlogD_c /cm^-3 (for B,C,D)
dN/dlogD_c /cm^-3 (for Dry and A)
Dry Period
Period A
Period B
Period C
Period D
BC core diameter (µm)
Fitting scavenging rate=0.95-0.60e^-10.24D_c
Fitting releasing rate=6.16-7.11e^-0.79D_c
Parameters of fitting lognormal size distribution for BC mass:
Dry A B C D
D0 0.21 0.21 0.16 0.18 0.23
σg 1.58 1.61 1.58 1.63 1.61

Figure3.

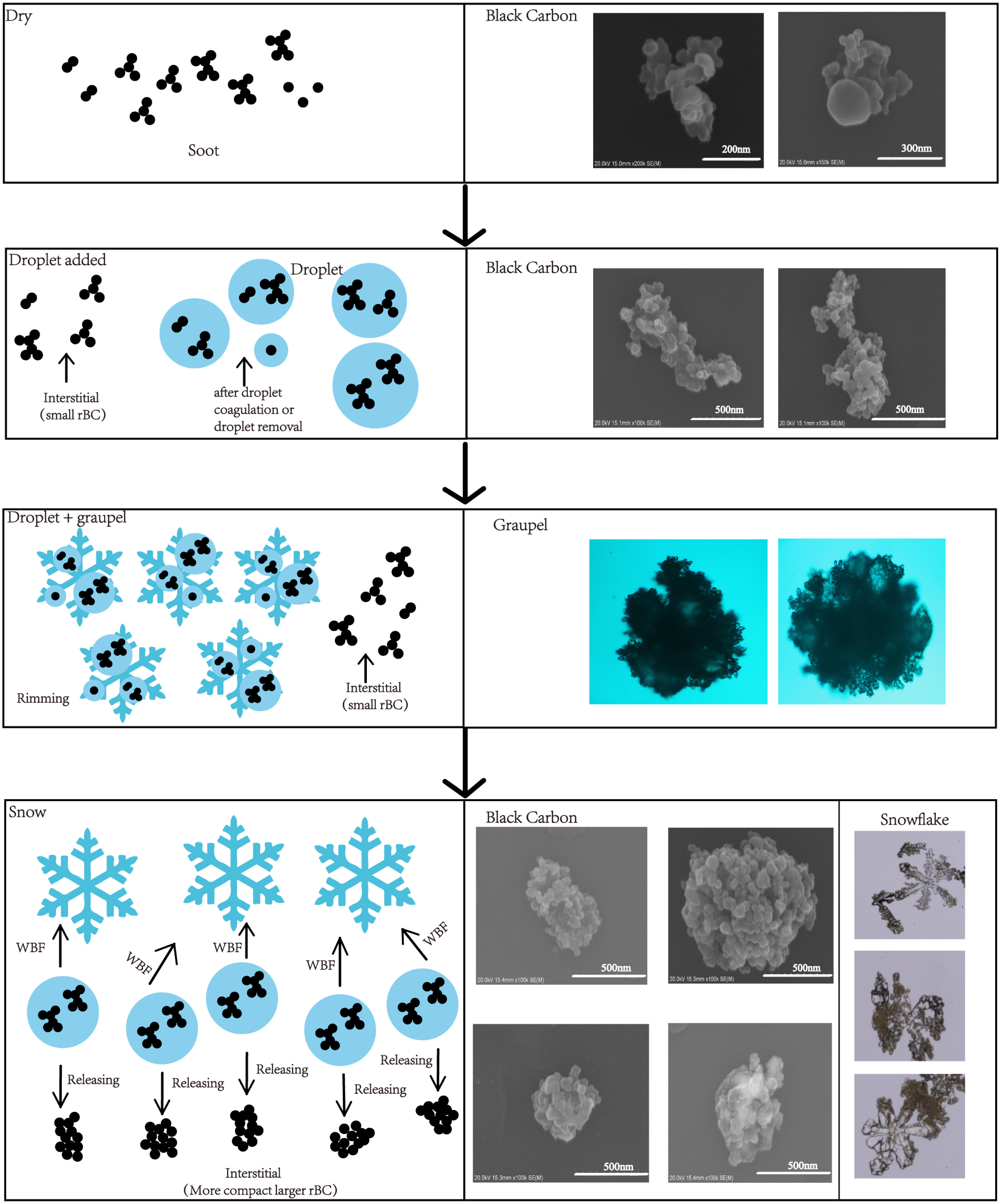

Dry
Soot
Black Carbon
200nm
300nm
Droplet added
Droplet
Interstitial
(small rBC)
after droplet
coagulation or
droplet removal
Black Carbon
500nm
500nm
Droplet + graupel
Rimming
Interstitial
(small rBC)
Graupel
Snow
WBF
Releasing
Interstitial
(More compact larger rBC)
Black Carbon
500nm
500nm
500nm
500nm
Snowflake